






Enhancing Cross-Modal Medical Image Segmentation through Compositionality

Aniek Eijpe^{1,2,3}, Valentina Corbetta^{2,3,4}, Kalina Chupetlovska², Regina Beets-Tan^{2,4}, and Wilson Silva^{2,3}

¹ University of Amsterdam, Amsterdam, The Netherlands
{[aniek.eijpe](mailto:aniek.eijpe@student.uva.nl)}@student.uva.nl

² Department of Radiology, The Netherlands Cancer Institute, Amsterdam, The Netherlands

³ AI Technology for Life, Department of Information and Computing Sciences, Department of Biology, Utrecht University, Utrecht, The Netherlands

⁴ GROW School for Oncology and Developmental Biology, Maastricht University Medical Center, Maastricht, The Netherlands

Abstract. Cross-modal medical image segmentation presents a significant challenge, as different imaging modalities produce images with varying resolutions, contrasts, and appearances of anatomical structures. We introduce compositionality as an inductive bias in a cross-modal segmentation network to improve segmentation performance and interpretability while reducing complexity. The proposed network is an end-to-end cross-modal segmentation framework that enforces compositionality on the learned representations using learnable von Mises-Fisher kernels. These kernels facilitate content-style disentanglement in the learned representations, resulting in compositional content representations that are inherently interpretable and effectively disentangle different anatomical structures. The experimental results demonstrate enhanced segmentation performance and reduced computational costs on multiple medical datasets. Additionally, we demonstrate the interpretability of the learned compositional features. Code and checkpoints will be publicly available at: <https://github.com/Trustworthy-AI-UU-NKI/Cross-Modal-Segmentation>.

Keywords: Cross-modal medical image segmentation · Disentangled Representation Learning · Compositionality

1 Introduction

Cross-modal medical image segmentation involves leveraging annotated images from one domain (e.g., Computed Tomography (CT)) to segment images in a different domain (e.g., Magnetic Resonance Imaging (MRI)) without available segmentation labels. This domain shift [18] poses numerous challenges, as different imaging modalities produce images with varying resolutions, contrasts, and noise levels. Additionally, anatomical structures may appear differently or may not be visible across modalities due to varying imaging principles and acquisition

parameters [16]. This heterogeneity makes it difficult to develop a segmentation model trained on for example CT that can effectively handle MRI as well.

In recent years, Disentangled Representation Learning (DRL) techniques have found significant application in the context of cross-modal image segmentation, often employed in a cross-modal translation setup [23,22,3,17,2,26]. DRL aims to learn general and meaningful representations that capture the underlying factors that generate the data variation [1,5]. By disentangling (i.e. separating) these factors, the representations become inherently more interpretable and generalizable to other domains [24]. In the context of cross-modal segmentation, most works focus on Content-Style Disentanglement (CSD) [4], separating the *content* from the *style* in two distinct representations. Generally, the style representations are considered domain-specific, while the content representations are viewed as domain-invariant and said to be shared across domains [12,11], although these definitions are not universally agreed upon [13].

Current methods require complex and large architectures and objective functions to bridge the gap between modalities [23,26,17,22], resulting in high computational costs. Moreover, defining and achieving proper and effective disentanglement between these representations is still a challenge. Multiple studies show that it is often unclear whether the learned representations are truly disentangled or not, showing information leakage between representations [16,13]. These challenges contribute to a lack of interpretability in current approaches.

Current methods require complex and large architectures and objective functions to bridge the gap between modalities [23,26,17,22], resulting in high computational costs. Moreover, defining and achieving proper and effective disentanglement between these representations is still a challenge. Multiple studies show that it is often unclear whether the learned representations are truly disentangled or not, showing information leakage between representations [16,13]. These challenges contribute to a lack of interpretability in current approaches.

We address these challenges by introducing compositionality as an inductive bias into an end-to-end cross-modal segmentation framework, aiming to reduce complexity and enhance interpretability. Compositionality refers to the notion that a representation as a whole should be composed of the representations of its parts [20]. This approach has been applied to numerous computer vision methods, demonstrating improvements in both robustness and explainability [21,10,14]. Our method enforces compositionality on the learned representations, which are modeled by learnable von Mises-Fisher (vMF) kernels [14]. These kernels effectively filter out style information. The resulting compositional, content representations contain only spatial information, additionally disentangling the anatomical structures from the background and each other, enhancing the interpretability of the learned representations. We argue that these content representations should not necessarily be shared across two different imaging modalities, since different modalities capture varying characteristics of anatomies [16]. Relying solely on domain-invariant information for segmentation may lead to omitting crucial data, as some relevant information may be domain-specific. Therefore, we define the content representations as compositional rather than

strictly domain-invariant. By implicitly modeling the style representations within these kernels, we remove the need for domain-specific style encoders, thereby reducing the complexity and consequentially computational costs.

The experimental results demonstrate enhanced performance and interpretability with reduced computational costs on an unpaired public cardiac CT & MRI dataset and abdominal multi-modal MRI dataset.

Summarizing, our key contributions are the following:

- We introduce compositionality as an inductive bias into a cross-modal segmentation framework, effectively disentangling the content representations.
- We reduce computational costs by implicitly modeling the style representations corresponding to several compositional components of human anatomy with learnable vMF kernels.
- We show enhanced cross-modal segmentation performance on two public, unpaired medical datasets and demonstrate the interpretability of the learned compositional content representations.

2 Methodology

We aim to develop a model to segment images from a target domain $y \in Y$, by using images from a source domain $x \in X$ with corresponding labels $m_x \in M$. Figure 1 displays our proposed framework. In the context of CSD, we adopt a two-stage disentanglement approach. Initially, our network roughly aligns the deep features \mathbf{Z}_x and \mathbf{Z}_y obtained by the two domain-specific encoders. Subsequently, the vMF kernels K_{vMF} filter out all remaining target-specific domain information to obtain the compositional, content representations \mathbf{Z}_{vMF} , which are used to obtain the final segmentation mask $\hat{m}_y \in M$.

Cross-modal translation To obtain a mapping between the source and the target domain, the network is trained to perform cross-modal translation from the source to the target domain and vice versa. E_x and E_y denote the domain-specific encoders, encoding the images of the source and target domain into deep features $\mathbf{Z}_x, \mathbf{Z}_y \in \mathbb{R}^{C_z \times H_z \times W_z}$, respectively. To translate the obtained representations to the other domain, the deep features \mathbf{Z}_x and \mathbf{Z}_y , are used by the generators G_y and G_x respectively, to generate *fake* images with the appearance of the respective domain but the content of the original domain. Since no paired data is available, a cross-cycle consistency loss [28] for both domains is used to learn the bi-directional mapping between the two domains.

$$\mathcal{L}_{cycle}^{x,y} = \mathbb{E}_{x,y} [\|G_{x,y}(E_{y,x}(G_{y,x}(E_{x,y}(\{x,y\})))) - \{x,y\}\|_1] \quad (1)$$

To enhance the quality of the generated images, an adversarial learning approach is adopted, with two domain discriminators D_x and D_y , acting on the source and target domain, respectively. These discriminators are trained to distinguish between real and fake images, while the generators attempt to produce images that

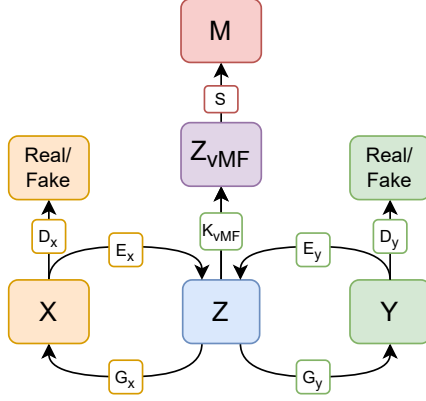


Fig. 1: Overview of the proposed framework. X and Y denote the source and target domain from which the encoders E_x and E_y extract the deep features into Z . From Z , the deep features can be translated to either domain with the generators G_x and G_y , or compositional representations Z_{vMF} can be obtained via the vMF kernels (K_{vMF}). From Z_{vMF} , the segmentation model S predicts the final segmentation masks. D_x and D_y denote the domain discriminators.

are indistinguishable from the real ones. The generator ($\mathcal{L}_{gen}^{x,y}$) and discriminator ($\mathcal{L}_{disc}^{x,y}$) losses are inspired by the Least Squares GAN (LSGAN) [15].

$$\mathcal{L}_{gen}^{x,y} = \frac{1}{2} \mathbb{E}_{y,x} [D_{x,y}(G_{x,y}(E_{y,x}(\{y,x\}))) - 1]^2 \quad (2)$$

$$\mathcal{L}_{disc}^{x,y} = \frac{1}{2} \mathbb{E}_{x,y} [(D_{x,y}(\{x,y\}) - 1)^2] + \frac{1}{2} \mathbb{E}_{y,x} [D_{x,y}(G_{x,y}(E_{y,x}(\{y,x\})))^2] \quad (3)$$

Learning compositional representations With the deep features \mathbf{Z}_y and the corresponding learnable vMF kernels, K_{vMF} , we obtain the compositional representations $\mathbf{Z}_{vMF} \in \mathbb{R}^{J \times H_z \times W_z}$. This process is depicted in Figure 2.

\mathbf{Z}_y can be viewed as a 2D map $H_z \times W_z$, with a feature vector $\mathbf{z}_{yi} \in \mathbb{R}^{C_z}$ on each position i . Following vMFNet’s principles [14], we model the feature representations \mathbf{Z}_y as a mixture of J von-Mises-Fisher distributions, where each distribution has a learnable mean. This learnable mean of distribution j is referred to as the vMF kernel $\boldsymbol{\mu}_j \in \mathbb{R}^{C_z}$. By calculating the vMF likelihood of each feature vector \mathbf{z}_{yi} following each vMF distribution $j \in \{1, \dots, J\}$, we obtain the compositional content representations $\mathbf{Z}_{vMF} \in \mathbb{R}^{J \times H_z \times W_z}$. The likelihood for each feature vector at position i following the distribution j is calculated as follows:

$$p(\mathbf{z}_{yi} | \boldsymbol{\mu}_j) = C(\sigma)^{-1} \cdot e^{\sigma \boldsymbol{\mu}_j^T \mathbf{z}_{yi}} \quad (4)$$

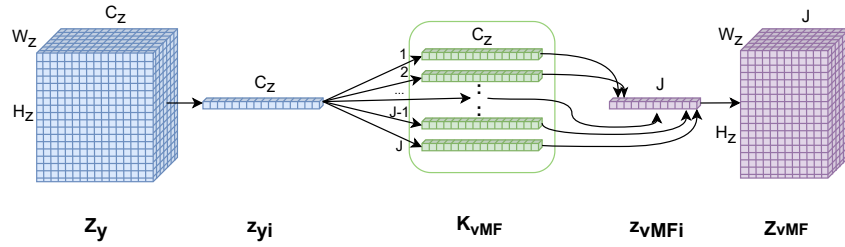


Fig. 2: Visual overview of learning a compositional representation \mathbf{Z}_{vMF} from the representation \mathbf{Z}_y containing the deep features of a single target image y .

where $\|\boldsymbol{\mu}_j\| = 1$ and $\|\mathbf{z}_{yi}\| = 1$. For tractability, the variance σ is fixed for all distributions. The obtained likelihoods are combined in $\mathbf{Z}_{vMF} \in \mathbb{R}^{J \times H_z \times W_z}$, indicating how much each kernel $j \in \{1, \dots, J\}$ is activated at each position i in the 2D feature map $H \times W$.

During training, the network optimizes these kernels to serve as cluster centers of the feature vectors, using the following cluster loss:

$$\mathcal{L}_{vMF}^y = \mathbb{E}_y \left[-(H \cdot W)^{-1} \sum_i \max_j \boldsymbol{\mu}_j^T \mathbf{z}_{yi} \right] \quad (5)$$

After training, the image feature vectors that are similar, activate the same kernels, have similar likelihoods, and are therefore clustered in the same channels of the compositional representation. These similar feature vectors are often induced by image patches that share semantic meaning [10].

Segmentation The segmentation model S is trained on the compositional content representations \mathbf{Z}_{vMF} , as these representations contain the spatial information. During training, only the labels of the source images are accessible. Therefore, we translate the source images to the target domain, and then from these translated images, the segmentation masks are obtained using the compositional features. The predicted segmentation masks are compared to the original segmentation labels of the source images using the Dice loss.

$$\mathcal{L}_{seg} = \mathbb{E}_x [\text{Dice}(m_x, S(K_{vMF}(E_y(G_y(E_x(x))))))] \quad (6)$$

3 Experiments

Datasets From the **Multi-Modality Whole Heart Segmentation (MM-WHS)** challenge [29] dataset, 320 CT and 320 MRI (b-SSFP) slices were extracted⁵ around the center of the left ventricular blood cavity along the long-

⁵ https://github.com/FupingWu90/CT_MR_2D_Dataset_DA

axis view [25] with annotated labels of the Myocardium (MYO), left ventricle blood cavity (LV), and right ventricle blood cavity (RV). From the **Combined Healthy Abdominal Organ Segmentation (CHAOS)** challenge [7,6], multi-modal abdominal MR sequence data (T1-DUAL and T2-SPIR) of healthy patients with segmentation labels of the liver parenchyma were utilized, with 647 T1 and 623 T2 scans. This dataset contains substantial variation in image content, including negative examples (i.e., images without the liver).

Baselines To evaluate the domain shift impact on segmentation performance, we employ a standard UNet [19] in two ways. The **UNet-NA**, trained on source data and tested on target data, serves as a lower bound. The **UNet-FS** is fully supervised on target data, serving as an upper performance bound. The **vMFNet** model, robust to images collected from different clinical centres [14], is tested against our large domain shift. The **DRIT+UNet** and **DRIT+RUNet** baselines use DRL in a two-stage cross-modal segmentation process: DRIT++ [11] learns to translate images between domains, then UNet and Residual UNet [8] are trained on synthetic target data. The **DDFSeg** [17] model, modified to validate on source labels, is an end-to-end CSD network using domain invariant features for segmentation. This modification aligns with the principle of not using target ground truth labels during training.

Implementation details The models are trained for 200 epochs using the Adam Optimizer [9] with a batch size of 4, a learning rate of 0.0001, and exponential decay rates $(\beta_1, \beta_2) = (0.5, 0.999)$. Algorithm 1 in the supplementary materials outlines the exact training strategy of our model. We empirically chose to set the number of vMF kernels to 10, which were initialized using Xavier initialization along with the rest of the network. Following Kortylewski *et al.* [10], we fixed the variance of the vMF distributions to 30. The model was trained and tested with 5-fold cross-validation, during which the model is validated with the Dice Similarity Coefficient (DSC) and the Learned Perceptual Image Patch Similarity (LPIPS) metric [27], measuring both segmentation performance and quality of generated images. After training, the models are evaluated with the DSC and the Average Symmetric Surface Distance (ASSD).

Cardiac segmentation Table 1 presents the quantitative results for segmenting the MYO, LV, and RV with CT as the target domain. The FS and NA baselines show a significant performance drop due to the domain shift. The vMFNet and DDF Segmentation network also perform poorly with this substantial modality shift. Our modification to the DDFSeg framework may have contributed to its reduced performance, as validating on true source labels provides a less precise estimate of the model’s performance on the target domain compared to validating on true target labels. Among the baselines, DRIT++ performs best, both with UNet and Residual UNet for second-stage segmentation. Overall, our proposed method outperforms all baselines. Supplementary

Table 1: Quantitative comparison on the MM-WHS dataset showing the mean and std over the different folds. The best performance is denoted in **Bold**.

MRI \rightarrow CT	MYO		LV		RV	
	DSC(%)	ASSD(mm)	DSC(%)	ASSD(mm)	DSC(%)	ASSD(mm)
UNet-FS	87.1 _{2.4}	1.3 _{0.3}	92.1 _{1.1}	1.4 _{0.2}	90.2 _{2.4}	1.8 _{0.4}
UNet-NA	5.3 _{4.7}	26.7 _{6.2}	37.2 _{23.4}	19.7 _{16.6}	25.4 _{22.5}	22.9 _{9.8}
vMFNet	2.3 _{1.4}	26.7 _{4.0}	52.4 _{15.3}	10.8 _{3.7}	40.4 _{9.7}	12.5 _{1.3}
DDFseg	24.5 _{5.8}	15.7 _{4.7}	39.1 _{3.1}	23.2 _{1.3}	24.2 _{14.2}	29.9 _{2.7}
DRIT+UNet	47.5 _{8.5}	5.3 _{2.0}	69.5 _{3.3}	6.0 _{1.4}	67.9 _{5.8}	5.5_{0.8}
DRIT+RUNet	58.4 _{3.8}	3.9 _{0.2}	75.1 _{3.1}	5.1 _{0.5}	71.5 _{2.5}	6.7 _{1.5}
Proposed	65.1_{4.8}	3.0_{0.6}	80.2_{4.7}	4.7_{1.5}	77.3_{3.6}	5.6 _{2.0}

Table 1 shows reverse direction results, and Figure 1 provides qualitative examples, demonstrating similar patterns. Introducing compositionality reduced training times significantly: 38 hours less than DRIT+UNet and DRIT+RUNet, and 16.5 hours less than DDFseg on the MM-WHS dataset.

Liver parenchyma segmentation Table 2 presents the quantitative results for segmenting the liver parenchyma with T1 and T2 as target domain. Generally, we see a similar pattern as with the cardiac segmentation. Notably though, with T2 \rightarrow T1, the drop in segmentation performance due to the domain gap is not as substantial. Our proposed method achieves the highest DSC in both directions, but the ASSD is substantially higher than the DRIT+UNet. Figure 1 in the supplementary material provides some qualitative results for both T1 target images and T2 target images.

Table 2: Quantitative comparison on the CHAOS dataset providing the mean and std over the different folds. The best performance is denoted in **Bold**.

Liver parenchyma	T2 \rightarrow T1		T1 \rightarrow T2	
	DSC(%)	ASSD(mm)	DSC(%)	ASSD(mm)
UNet-FS	89.1 _{1.8}	3.4 _{0.9}	88.5 _{4.5}	4.5 _{1.9}
UNet-NA	62.9 _{4.0}	19.3 _{7.7}	25.2 _{11.6}	31.3 _{8.5}
vMFNet	40.9 _{9.5}	29.5 _{12.4}	25.6 _{9.6}	22.0 _{2.4}
DDFseg	24.1 _{11.7}	69.3 _{17.3}	17.0 _{9.3}	69.6 _{8.4}
DRIT+UNet	62.8 _{5.9}	17.8_{5.9}	54.1 _{9.0}	15.6_{3.3}
DRIT+RUNet	58.8 _{7.4}	29.3 _{9.3}	53.9 _{4.2}	23.2 _{2.4}
Proposed	64.6_{4.6}	23.2 _{5.3}	66.3_{5.1}	19.1 _{5.7}

Compositional representations Figure 3 shows visual results of the learned compositional representations. The first three rows illustrate the network’s ability to learn components representing anatomical structures like the MYO, LV,

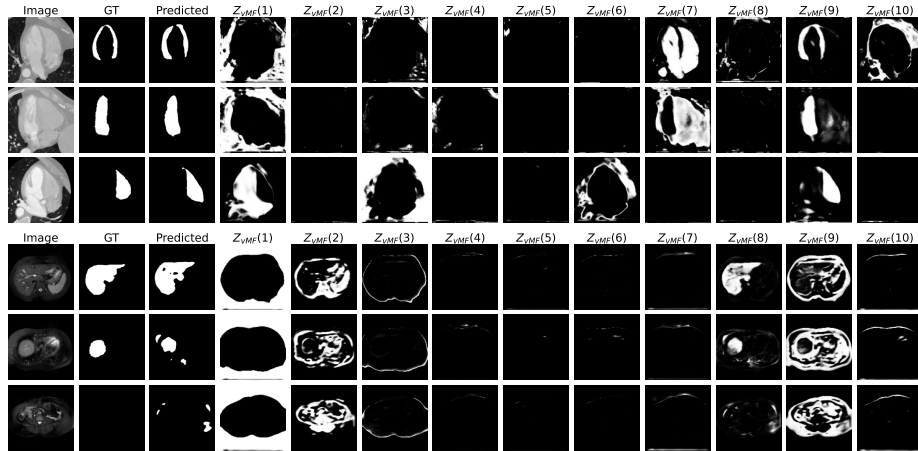


Fig. 3: Visual results of our proposed method segmenting the MYO, LV, RV, with target CT images, and the liver parenchyma with target T2-SPIR Images, with the 10 different channels of the compositional representation.

RV, other heart parts, and the chest wall. Despite missing some fine details, these interpretable representations achieve good segmentation performance. For liver parenchyma segmentation, a similar pattern is observed. However, the channels that are primarily activated by the liver parenchyma show merged activations. We suspect that due to the high variability in image content, the model struggles to find reliable style representations for the liver. Consequently, some non-liver patches activate channel 8, causing the network to produce a segmentation mask with several small artifacts even when no liver parenchyma is present in the image. These artifacts elevate the ASSD despite good DSC. A post-processing step, retaining only the largest connected component in each predicted mask, can mitigate these artifacts.

4 Conclusions

We presented a novel end-to-end cross-modal segmentation framework that leverages images and segmentation labels from an annotated-rich domain to segment images from another, annotated poor domain. We introduced compositionality into a DRL network to address the lack of interpretability and high computational costs in the current models. By enforcing the learned representations to be compositional, we effectively disentangle style features from content features. These content features are further disentangled, separating the representations of different anatomical structures. The qualitative and quantitative experiments demonstrated enhanced performance on cardiac CT-MRI MYO, LV, and RV segmentation, outperforming cross-modal segmentation baselines employing disentangled representations. Moreover, our network showed an increase in the DSC

for cross-modal MRI liver parenchyma segmentation. Additionally, we reduced complexity, and thereby vastly decreased computational costs. Lastly, the interpretable nature of the learned compositional representations provided valuable insights into the segmentation process. Future research will focus on handling negative examples and expanding to multi-class segmentation to further improve compositional representations and consequently, segmentation performance.

Acknowledgments. Research at the Netherlands Cancer Institute is supported by grants from the Dutch Cancer Society and the Dutch Ministry of Health, Welfare and Sport. The authors would like to acknowledge the Research High Performance Computing (RHPC) facility of the Netherlands Cancer Institute (NKI).

Disclosure of Interests. The authors have no competing interests to declare that are relevant to the content of this article.

References

1. Bengio, Y., Courville, A., Vincent, P.: Representation learning: A review and new perspectives. *IEEE transactions on pattern analysis and machine intelligence* **35**(8), 1798–1828 (2013)
2. Chen, J., Zhang, Z., Xie, X., Li, Y., Xu, T., Ma, K., Zheng, Y.: Beyond mutual information: Generative adversarial network for domain adaptation using information bottleneck constraint. *IEEE Transactions on Medical Imaging* **41**(3), 595–607 (2021)
3. Chen, X., Lian, C., Wang, L., Deng, H., Kuang, T., Fung, S.H., Gateno, J., Shen, D., Xia, J.J., Yap, P.T.: Diverse data augmentation for learning image segmentation with cross-modality annotations. *Medical image analysis* **71**, 102060 (2021)
4. Gatys, L.A., Ecker, A.S., Bethge, M.: Image style transfer using convolutional neural networks. In: *Proceedings of the IEEE conference on computer vision and pattern recognition*. pp. 2414–2423 (2016)
5. Higgins, I., Amos, D., Pfau, D., Racaniere, S., Matthey, L., Rezende, D., Lerchner, A.: Towards a definition of disentangled representations. *arXiv preprint arXiv:1812.02230* (2018)
6. Kavur, A.E., Gezer, N.S., Barış, M., Aslan, S., Conze, P.H., Groza, V., Pham, D.D., Chatterjee, S., Ernst, P., Özkan, S., Baydar, B., Lachinov, D., Han, S., Pauli, J., Isensee, F., Perkonigg, M., Sathish, R., Rajan, R., Sheet, D., Dovletov, G., Speck, O., Nürnberger, A., Maier-Hein, K.H., Bozdağı Akar, G., Ünal, G., Dicle, O., Selver, M.A.: CHAOS Challenge - combined (CT-MR) healthy abdominal organ segmentation. *Medical Image Analysis* **69**, 101950 (Apr 2021). <https://doi.org/https://doi.org/10.1016/j.media.2020.101950>, <http://www.sciencedirect.com/science/article/pii/S1361841520303145>
7. Kavur, A.E., Selver, M.A., Dicle, O., Barış, M., Gezer, N.S.: CHAOS - Combined (CT-MR) Healthy Abdominal Organ Segmentation Challenge Data (Apr 2019). <https://doi.org/10.5281/zenodo.3362844>, <https://doi.org/10.5281/zenodo.3362844>
8. Kerfoot, E., Clough, J., Oksuz, I., Lee, J., King, A.P., Schnabel, J.A.: Left-ventricle quantification using residual u-net. In: *Statistical Atlases and Computational Models of the Heart. Atrial Segmentation and LV Quantification Challenges: 9th International Workshop, STACOM 2018, Held in Conjunction with MICCAI 2018,*

- Granada, Spain, September 16, 2018, Revised Selected Papers 9. pp. 371–380. Springer (2019)
9. Kingma, D.P., Ba, J.: Adam: A method for stochastic optimization. arXiv preprint arXiv:1412.6980 (2014)
 10. Kortylewski, A., He, J., Liu, Q., Yuille, A.L.: Compositional convolutional neural networks: A deep architecture with innate robustness to partial occlusion. In: Proceedings of the IEEE/CVF Conference on Computer Vision and Pattern Recognition. pp. 8940–8949 (2020)
 11. Lee, H.Y., Tseng, H.Y., Mao, Q., Huang, J.B., Lu, Y.D., Singh, M., Yang, M.H.: Drit++: Diverse image-to-image translation via disentangled representations. *International Journal of Computer Vision* **128**, 2402–2417 (2020)
 12. Liu, M.Y., Breuel, T., Kautz, J.: Unsupervised image-to-image translation networks. *Advances in neural information processing systems* **30** (2017)
 13. Liu, X., Sanchez, P., Thermos, S., O’Neil, A.Q., Tsaftaris, S.A.: Learning disentangled representations in the imaging domain. *Medical Image Analysis* **80**, 102516 (2022)
 14. Liu, X., Thermos, S., Sanchez, P., O’Neil, A.Q., Tsaftaris, S.A.: vmfnet: Compositionality meets domain-generalised segmentation. In: International Conference on Medical Image Computing and Computer-Assisted Intervention. pp. 704–714. Springer (2022)
 15. Mao, X., Li, Q., Xie, H., Lau, R.Y., Wang, Z., Paul Smolley, S.: Least squares generative adversarial networks. In: Proceedings of the IEEE international conference on computer vision. pp. 2794–2802 (2017)
 16. Ouyang, J., Adeli, E., Pohl, K.M., Zhao, Q., Zaharchuk, G.: Representation disentanglement for multi-modal brain mri analysis. In: Information Processing in Medical Imaging: 27th International Conference, IPMI 2021, Virtual Event, June 28–June 30, 2021, Proceedings 27. pp. 321–333. Springer (2021)
 17. Pei, C., Wu, F., Huang, L., Zhuang, X.: Disentangle domain features for cross-modality cardiac image segmentation. *Medical Image Analysis* **71**, 102078 (2021)
 18. Quinonero-Candela, J., Sugiyama, M., Schwaighofer, A., Lawrence, N.D.: *Dataset shift in machine learning*. Mit Press (2008)
 19. Ronneberger, O., Fischer, P., Brox, T.: U-net: Convolutional networks for biomedical image segmentation. In: Medical Image Computing and Computer-Assisted Intervention–MICCAI 2015: 18th International Conference, Munich, Germany, October 5–9, 2015, Proceedings, Part III 18. pp. 234–241. Springer (2015)
 20. Stone, A., Wang, H., Stark, M., Liu, Y., Scott Phoenix, D., George, D.: Teaching compositionality to cnns. In: Proceedings of the IEEE conference on computer vision and pattern recognition. pp. 5058–5067 (2017)
 21. Tokmakov, P., Wang, Y.X., Hebert, M.: Learning compositional representations for few-shot recognition. In: Proceedings of the IEEE/CVF International Conference on Computer Vision. pp. 6372–6381 (2019)
 22. Wang, R., Zheng, G.: Unsupervised cross-modality cardiac image segmentation via disentangled representation learning and consistency regularization. In: Machine Learning in Medical Imaging: 12th International Workshop, MLMI 2021, Held in Conjunction with MICCAI 2021, Strasbourg, France, September 27, 2021, Proceedings 12. pp. 517–526. Springer (2021)
 23. Wang, R., Zheng, G.: Cycmis: Cycle-consistent cross-domain medical image segmentation via diverse image augmentation. *Medical Image Analysis* **76**, 102328 (2022)
 24. Wang, X., Chen, H., Tang, S., Wu, Z., Zhu, W.: Disentangled representation learning. arXiv preprint arXiv:2211.11695 (2022)

25. Wu, F., Zhuang, X.: Cf distance: a new domain discrepancy metric and application to explicit domain adaptation for cross-modality cardiac image segmentation. *IEEE Transactions on Medical Imaging* **39**(12), 4274–4285 (2020)
26. Xie, Q., Li, Y., He, N., Ning, M., Ma, K., Wang, G., Lian, Y., Zheng, Y.: Unsupervised domain adaptation for medical image segmentation by disentanglement learning and self-training. *IEEE Transactions on Medical Imaging* (2022)
27. Zhang, R., Isola, P., Efros, A.A., Shechtman, E., Wang, O.: The unreasonable effectiveness of deep features as a perceptual metric. In: *Proceedings of the IEEE conference on computer vision and pattern recognition*. pp. 586–595 (2018)
28. Zhu, J.Y., Park, T., Isola, P., Efros, A.A.: Unpaired image-to-image translation using cycle-consistent adversarial networks. In: *Proceedings of the IEEE international conference on computer vision*. pp. 2223–2232 (2017)
29. Zhuang, X., Li, L., Payer, C., Štern, D., Urschler, M., Heinrich, M.P., Oster, J., Wang, C., Smedby, Ö., Bian, C., et al.: Evaluation of algorithms for multi-modality whole heart segmentation: an open-access grand challenge. *Medical image analysis* **58**, 101537 (2019)